NeuroImage: Clinical 24 (2019) 102098

Contents lists available at ScienceDirect

NeuroImage: Clinical

journal homepage: www.elsevier.com/locate/ynicl

A longitudinal fixel-based analysis of white matter alterations in patients with Parkinson's disease

Yi-Ai Rau[a,1], Shi-Ming Wang[b,1], Jacques-Donald Tournier[c], Sung-Han Lin[b], Chin-Song Lu[d,e,f], Yi-Hsin Weng[d,e,f], Yao-Liang Chen[g,h], Shu-Hang Ng[b,h], Shao-Wen Yu[a], Yi-Ming Wu[b,h], Chih-Chien Tsai[b,i], Jiun-Jie Wang[b,g,i,j,*]

[a] Division of Chinese Acupuncture and Traumatology, Center for Traditional Chinese Medicine, Chang Gung Memorial Hospital, Linkou Branch, Taoyuan, Taiwan
[b] Department of Medical Imaging and Radiological Sciences, Chang Gung University, Taoyuan, Taiwan
[c] Division of Imaging Sciences & Biomedical Engineering, King's College London, London, United Kingdom
[d] Neuroscience Research Center, Chang Gung Memorial Hospital, Linkou Branch, Taoyuan, Taiwan
[e] Division of Movement Disorders, Department of Neurology, Chang Gung Memorial Hospital, Linkou Branch, Taoyuan, Taiwan
[f] School of Medicine, Chang Gung University, Taoyuan, Taiwan
[g] Department of Diagnostic Radiology, Chang Gung Memorial Hospital, Keelung Branch, Keelung, Taiwan
[h] Department of Medical Imaging and Intervention, Chang Gung Memorial Hospital, Linkou Branch, Taoyuan, Taiwan
[i] Healthy Aging Research Center, College of Medicine, Chang Gung University, Taoyuan, Taiwan
[j] Medical Imaging Research Center, Institute for Radiological Research, Chang Gung University/Chang Gung Memorial Hospital, Taoyuan, Taiwan

ARTICLE INFO

Keywords:
Parkinson's disease
Diffusion MRI
Fixel-based analysis
White matter
Axon degeneration
Aging

ABSTRACT

Introduction: Disruption to white matter pathways is an important contributor to the pathogenesis of Parkinson's disease. Fixel-based analysis has recently emerged as a useful fiber-specific tool for examining white matter structure. In this longitudinal study, we used Fixel-based analysis to investigate white matter changes occurring over time in patients with Parkinson's disease.

Methods: Fifty patients with idiopathic Parkinson's disease (27 men and 23 women; mean age: 61.8 ± 6.1 years), were enrolled. Diffusion-weighted imaging and clinical examinations were performed at three different time points (baseline, first follow-up [after a mean of 24 ± 2 months], and second follow-up [after a mean of 40 ± 3 months]). Additional 76 healthy control subjects (38 men and 38 women; mean age: 62.3 ± 5.5 years) were examined at baseline. The following fixel-based metrics were obtained: fiber density (FD), fiber bundle cross-section (FC), and a combined measure of both (FDC). Paired comparisons of metrics between three different time points were performed in patients. Linear regression was implemented between longitudinal changes of fixel-based metrics and the corresponding modifications in clinical parameters. A family-wise error corrected $p < 0.05$ was considered statistically significant.

Results and Discussions: Early degeneration in the splenium of corpus callosum was identified as a typical alteration of Parkinson's disease over time. At follow-up, we observed significant FDC reductions compared with baseline in white matter, noticeably in corpus callosum; tapetum; cingulum, posterior thalamic radiation, corona radiata, and sagittal stratum. We also identified significant FC decreases that reflected damage to white matter structures involved in Parkinson's disease -related pathways. Fixel-based metrics were found to relate with a deterioration of 39-item Parkinson's Disease Questionnaire, Unified Parkinson's Disease Rating Scale and activity of daily living. A Parkinson's disease -facilitated aging effect was observed in terms of white matter disruption.

Conclusion: This study provides a thorough fixel-based profile of longitudinal white matter alterations occurring

Abbreviations: PD, Parkinson's disease; FBA, fixel-based analysis; FD, fiber density; FC, fiber bundle cross-section; FDC, fiber density and cross-section; FA, fractional anisotropy; MD, mean diffusivity; DTI, diffusion tensor imaging; UPDRS, Unified Parkinson's Disease Rating Scale; MHY, modified Hoehn and Yahr scale; ADL, Schwab and England activities of daily living; MMSE, Mini-Mental State Examination; CDR, Clinical Dementia Rating; PDQ39, 39-item Parkinson's Disease Questionnaire; FOD, fiber orientations distribution; MSMT-CSD, multi-shell multi-tissue constrained spherical deconvolution; CFE, connectivity-based fixel enhancement

* Corresponding author at: Department of Medical Imaging and Radiological Sciences, Chang Gung University, 259 WenHua 1st road, TaoYuan county 333, Taoyuan, Taiwan.
E-mail address: jwang@mail.cgu.edu.tw (J.-J. Wang).
[1] These authors contributed equally to this work.

https://doi.org/10.1016/j.nicl.2019.102098
Received 23 May 2019; Received in revised form 1 October 2019; Accepted 16 November 2019
Available online 18 November 2019

in patients with Parkinson's disease and new evidence of FC as an important role in white matter degeneration in this setting.

1. Introduction

Parkinson's disease (PD) is a progressive neurodegenerative disease pathologically characterized by the selective loss of pigmented dopaminergic neurons in the substantia nigra and the presence of abnormal inclusions (Lewy bodies and Lewy neurites) widespread in the surviving neurons (Damier et al., 1999). Postmortem human studies have shown a putative progression of Lewy bodies pathology from the basal prosencephalon to the mesocortex and further to the neocortex (Braak et al., 2003). In addition to the loss of dopaminergic neurons, disruption to white matter pathways is an important contributor to the pathogenesis of PD (Bohnen and Albin, 2011; Tagliaferro and Burke, 2016).

Previous structural MRI studies in patients with PD have mainly reported brain atrophy (Atkinson-Clement et al., 2017), with limited evidence of PD-specific microstructural alterations (Brooks, 2010). In recent years, diffusion tensor imaging (DTI) has emerged as a valuable tool to investigate white matter damage in PD—with a decreased diffusion directionality (i.e., fractional anisotropy [FA]) being evident in the frontal white matter, superior longitudinal fasciculus, corpus callosum, and internal and external capsules (Kendi et al., 2008; Zhan et al., 2012). A recent meta-analysis confirmed that PD is characterized by a significant decrease in FA as well as by an increased mean diffusivity (MD) in the corpus callosum (Atkinson-Clement et al., 2017).

Unfortunately, DTI studies in white matter have been inconsistent in result and varied in methods (Atkinson-Clement et al., 2017; Bohnen and Albin, 2011). For example, FA in cingulum was reported to be increased (Hsu et al., 2010), decreased (Jang et al., 2016), or stable (Michielse et al., 2010) as the subjects aged. The controversy may be potentially as a result from either an imprecise representations and projections with inadequate modeling (Bach et al., 2014), or complex white matter fiber configurations, such as crossing (Assaf and Pasternak, 2008; Raffelt et al., 2015). In order to circumvent these issues, fixel-based analysis (FBA) was proposed to investigate white matter changes (Raffelt et al., 2015).

The term fixel denotes a specific fiber population within a voxel (Raffelt et al., 2015). FBA is a novel approach that allows determining fiber density (FD), fiber bundle cross-section (FC), or the combination of both (FDC) (Raffelt et al., 2017). These metrics might provide unique information that may help to understand the pathophysiology of white matter changes (Raffelt et al., 2017). The changes of fiber density (FD) can be related to an alteration of the intra-axonal volume. A decrease in intra-axonal volume may be ascribed to a degeneration of axon. The fiber bundle cross-section (FC) metric reflects the cross-sectional size of fiber bundles. The reduction of FC may occur as a consequence of white

Table 1
General characteristics of the study subjects.

	HC (n = 76)	PD (n = 50)			
		Baseline	First follow-up	Second follow-up	p-value*
		I	II	III	IV*
Sex (men/women)	38/38	27/23			
Age (yr)	62.3 ± 5.5	61.8 ± 6.1			
Disease duration (yr)	N/A	6.3 ± 5.0			
Education (yr)	12 ± 4.2	10 ± 4.5			
MHY	N/A	1.9 ± 0.8 (1-3, median = 2)	2.1 ± 1.0[a] (1-4, median = 2)	2.4 ± 1.0 [e g] (1-4, median = 2.5)	< 0.001
UPDRS	N/A	28.1 ± 15.0	32.3 ± 18.6 [a]	38.4 ± 22.3 [e g]	< 0.001
I	N/A	1.7 ± 2.0	1.6 ± 1.3	2.1 ± 1.9 [c]	0.135
II	N/A	6.8 ± 4.4	9.8 ± 6.1 [b]	11.3 ± 7.1 [d g]	< 0.001
III	N/A	18.1 ± 10.4	19.4 ± 12.1	23.2 ± 15.1 [e f]	< 0.001
IV	N/A	1.6 ± 1.9	1.5 ± 2.3	1.8 ± 2.1	0.519
ADL(%)	N/A	88.8 ± 6.9	83.6 ± 11.6 [b]	79.2 ± 15.0 [e g]	< 0.001
PDQ39	N/A	22.9 ± 19.9	35.8 ± 23.9 [b]	36.8 ± 25.6 [g]	< 0.001
MMSE	29.1 ± 1.1	27.4 ± 2.7	28.1 ± 3.5	27.9 ± 2.7	0.166
CDR	N/A	0.2 ± 0.2 (0-0.5, median = 0.5)	0.3 ± 0.3 (0-1, median = 0.5)	0.4 ± 0.3 [f] (0-1, median = 0.5)	0.002

Values are presented as means ± standard deviations, unless otherwise indicated.
HC = healthy control, PD = Parkinson's disease, N/A = data not available, UPDRS = Unified Parkinson's Disease Rating Scale, MHY = modified Hoehn and Yahr scale, MMSE = Mini-Mental State Examination, CDR = Clinical Dementia Rating, ADL = Schwab and England activities of daily living, PDQ39 = 39-item Parkinson's Disease Questionnaire
*Analysis performed with one-way repeated measures ANOVA.
[a] p value < 0.05 between the first follow-up assessment and baseline
[b] p value < 0.001 between the first follow-up assessment and baseline
[c] p value < 0.05 between the second and first follow-up assessments
[d] p value < 0.01 between the second and first follow-up assessments
[e] p value < 0.001 between the second and first follow-up assessments
[f] p value < 0.01 between the second follow-up assessment and baseline
[g] p value < 0.001 between the second follow-up assessment and baseline

matter atrophy – characterized by narrowing of the extra-axonal space, following the axonal loss (Raffelt et al., 2017) or hypomyelination and disorganization of axons (Malhotra et al., 2019). A combined measure of fiber density and fiber-bundle cross-section (FDC) provides a more comprehensive measure of white matter changes – because both macroscopic (FC) and microscopic (FD) effects on overall fiber density are taken into account (Raffelt et al., 2017).

Previous imaging studies of PD have been limited by their cross-sectional design (Bohnen and Albin, 2011; Taylor et al., 2018). Because neurodegeneration is typically characterized by a progressive course, the use of serial imaging examinations allows investigating brain modifications over time. Starting from these premises and by taking advantage of the novel FBA framework we designed the current longitudinal study to shed more light on white matter changes occurring over time in patients with PD.

2. Materials and methods

The study protocol complied with the tenets of the Declaration of Helsinki and was approved by the Institutional Review Board of the Chang Gung Memorial Hospital. All participants gave their written informed consent.

2.1. Study participants

Fifty patients with idiopathic PD (27 men and 23 women; mean age: 61.8 ± 6.1 years), and 76 age range-matched and sex-balanced healthy control subjects (38 men and 38 women; mean age: 62.3 ± 5.5 years) were examined (Table 1). All of them have been involved in a larger DTI study conducted at the Chang Gung Memorial Hospital (Linkou, Taiwan) between 2012 and 2016—whose results have been previously published (Lu et al., 2016).

Patients were deemed eligible if they met the following criteria: (1) diagnosis of PD according the United Kingdom Parkinson's Disease Society Brain Bank Clinical Diagnostic Criteria (Hughes et al., 1992) and (2) Hoehn and Yahr stages 1 − 3; (3) had performed diffusion-weighted imaging and clinical examinations at three different time points (baseline, first follow-up [after a mean of 24 ± 2 months] and second follow-up [after a mean of 40 ± 3 months]). The exclusion criteria were as follows: (1) presence of intracranial structural abnormalities (diagnosed on CT or MRI) potentially resulting in cognitive deficits; (2) positive history of intracranial surgery (including deep brain stimulation); (3) a DSM-IV diagnosis of dementia or other neuropsychiatric disorders; and (4) major physical illnesses. The following clinical measures were obtained from PD patients: Unified Parkinson's Disease Rating Scale (UPDRS) (Fahn et al., 1987) -off-drug state, modified Hoehn and Yahr scale (MHY) (Goetz et al., 2004), Schwab and England activities of daily living (ADL) (Schwab et al., 1969), Mini-Mental State Examination (MMSE) (Tombaugh and McIntyre, 1992), Clinical Dementia Rating (CDR) (Morris, 1993), and 39-item Parkinson's Disease Questionnaire (PDQ39) (Peto et al., 1995). Two senior neurologists (CS Lu and YH Weng, with 29 and 22 years of experience, respectively) confirmed the diagnosis and clinical measures. The healthy control subjects were solely examined with diffusion-weighted imaging at baseline and no follow-up data are available.

2.2. Image acquisition

Magnetic Resonance Images were acquired with a 3T scanner (Trio Magnetom; Siemens, Erlangen, Germany). A head fixation pad was used to minimize motion-related artifacts. T2-weighted turbo spin-echo, T2-weighted Flow Attenuated Inversion Recovery, and T1-weighted

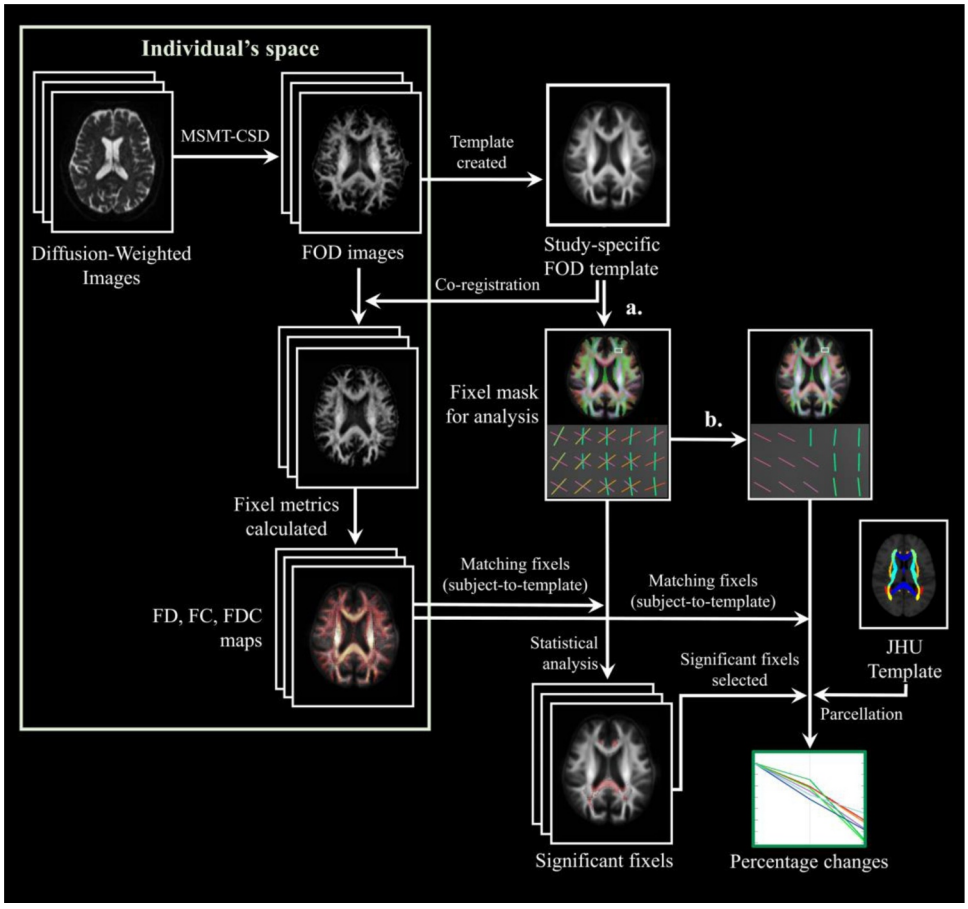

Fig. 1. Flowchart of imaging analysis. The procedures required for fixel-based analysis included (1) preprocessing, (2) estimation for distribution of fiber orientation (FOD), (3) development of study-specific templates, (4) creation of an analysis fixel mask, (5) Matching of the fixels from each subject to the template fixels (analysis fixel mask), and (6) calculation of fixel-based metrics. For white matter parcellation, we followed the procedure previously described by Lo et al. using the JHU DTI-based white matter atlas. (a): Selection of FOD amplitudes larger than 0.06 to create an analysis fixel mask of white matter. (b): Selection of the highest FOD amplitudes to create an analysis fixel mask with only major direction. MSMT-CSD: multi-shell multi-tissue constrained spherical deconvolution; FOD: fiber orientation distribution; FD: fiber density; FC: fiber-bundle cross-section; FDC: fiber density and cross-section; JHU: Johns Hopkins University.

Magnetization Prepared Rapid Acquisition Gradient recalled Echo (T1-MPRAGE) images were acquired to rule out intracranial structural abnormalities. Three senior neuroradiologists (SH Ng, YL Chen, and YM Wu, with 28, 20, and 10 years of experience, respectively) blinded to clinical data independently interpreted all MR images. Imaging parameters were as follows: repetition time (TR)/echo time (TE)/inversion time/flip angle = 2000 ms/2.63 ms/900 ms/9°, number of slices = 160, slice thickness = 1 mm, matrix size = 224 × 256, field of view = 224 × 256 mm^2, and acquisition time = 4 min and 8 s.

Multi-shell diffusion-weighted images were acquired using a spin-echo echo planar imaging (EPI) sequence with the following settings: TR/TE = 5700 ms/108 ms, voxel size = 2 × 2 × 3 mm^3, flip angle = 90°, matrix size = 96 × 96, field of view = 192 × 192 mm^2. Forty slices were acquired to cover the brain above the cerebellum. Diffusion-weighted gradients were applied along 30 non-collinear directions using b-values of 0, 1000, 2000, and 3000 s/mm^2. The averaged signal-to-noise ratio in images of b0 is 19.21 ± 4.5

2.3. Image analysis

2.3.1. Fixel-based analysis

FBA was implemented using MRtrix3 in accordance with the recommended procedures (Raffelt et al., 2017). The following operations were performed in the preprocessing steps: (1) Marchenko-Pastur principal component analysis (MP-PCA) denoising (Veraart et al., 2016); (2) Gibbs ringing removal (Kellner et al., 2016); (3) motion and distortion correction (Andersson and Sotiropoulos, 2015; Andersson and Sotiropoulos, 2016); and (4) bias field correction (Tustison et al., 2010). The fiber orientation distribution (FOD) within each imaging voxel was estimated using multi-tissue constrained spherical deconvolution (Jeurissen et al., 2014). Subsequently, a study-specific template was created by spatial normalization in all of the subjects using symmetric diffeomorphic non-linear transformation FOD-based registration. A group-averaged FOD template of patients with PD was created at baseline for the purpose of longitudinal comparison. Another FOD template including all patients with PD and healthy control subjects was developed at baseline to allow for inter-group comparisons (Raffelt et al., 2011). Fixel-specific measures of both fiber density (FD) and fiber bundle cross-section (FC) were calculated within each voxel. We also derived a combined measure (termed FDC) by multiplying FD and FC (Raffelt et al., 2017) (Fig. 1).

2.3.2. White matter parcellation

The modifications of fixel-based metrics were calculated for the

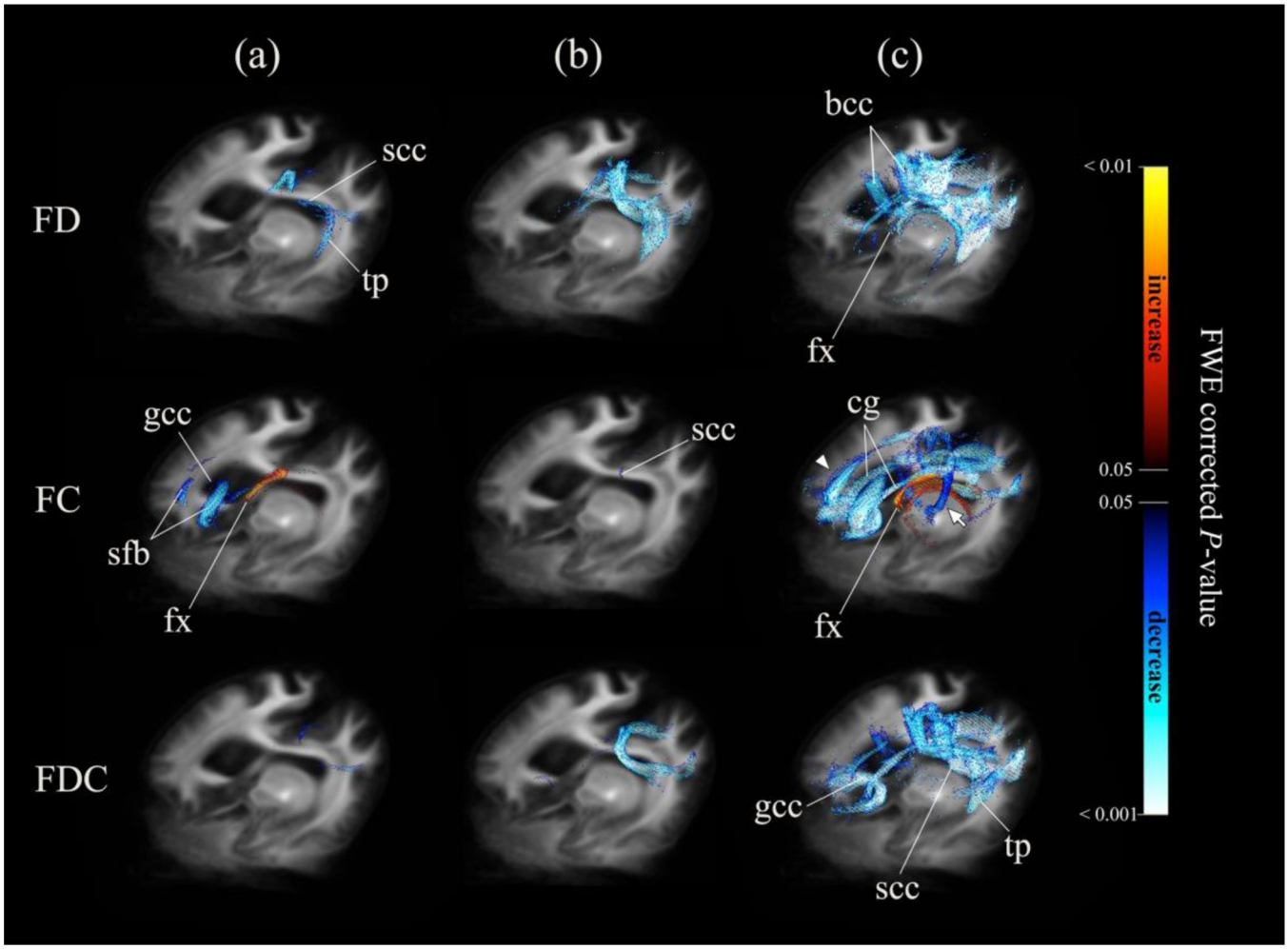

Fig. 2. Significant changes in fixel-based metrics over time. Areas of significant changes in fiber density (FD), fiber-bundle cross-section (FC), and fiber density and cross-section (FDC) during different study periods displayed stereoscopically in the superior left frontal view. Significant fixels (family-wise error corrected $p < 0.05$) were illustrated using streamline points and colored according to p-values. Cold colors denote reduction, whereas warm colors denote increase. Column (a): Significant areas between baseline and first follow-up; Column (b): Significant areas between first follow-up and second follow-up; Column (c): Significant areas between baseline and second follow-up. FD: fiber density; FC: fiber-bundle cross-section; FDC: fiber density and cross-section; scc: splenium of corpus callosum; tp: tapetum; bcc: body of corpus callosum; fx: fornix; gcc; genu of corpus callosum; sfb: superior frontal blade; cg: cingulum; Arrow head: left superior frontal white matter changes; Arrow: hyperdirect pathway.

major fiber bundles in each parcellated brain region. We followed the parcellated procedure originally described by Lo et al. (2010) using the Johns Hopkins University (JHU) DTI-based white matter atlas (ICBM-DTI-81 white matter labels atlas) (Mori et al., 2008). The JHU template was applied to identify the regions in white matter for determining how FDC changes could stem from variations in either FD or FC. In each region of interest, fixels showing a significant decrease in FDC between the second follow-up and baseline were identified, from which both FD and FC were extracted. The percentage changes and average of metrics in these fixels were subsequently calculated.

Because of image coverage, the following regions were excluded from the analysis: middle cerebellar peduncle, pontine crossing tract, medial lemniscus, and inferior cerebellar peduncle.

2.3.3. Voxel-based analysis

All processing followed Grazioplene et al. using MRtrix3 commands (Grazioplene et al., 2018). The pre-processing procedures included: (1) Marchenko-Pastur principal component analysis (MP-PCA) denoising (Veraart et al., 2016); (2) Gibbs ringing removal (Kellner et al., 2016); (3) motion and distortion correction (Andersson and Sotiropoulos, 2015; Andersson and Sotiropoulos, 2016); and (4) bias field correction (Tustison et al., 2010). Diffusion tensor parameters were estimated in each subject using the weighted linear least squares estimator (Veraart et al., 2013). Tensor-derived metrics—including fractional anisotropy (FA) and mean diffusivity (MD)—were calculated. Data were normalized to a study-specific FOD template based on warps generated from FOD-based registration in FBA.

2.4. Statistical analysis

2.4.1. Demographic description

Differences in clinical parameters between baseline and the two follow-up assessments were examined using one-way repeated measures analysis of variance (ANOVA). Statistical analysis of demographic descriptions was performed in the SPSS statistical package (version 24; IBM, Armonk, NY, USA). The threshold for statistical significance was at $p < 0.05$.

2.4.2. Statistical analysis of images

Statistical analyses of images were performed in MRtrix3. We used family-wise error-corrected p values to account for multiple comparisons (Nichols and Holmes, 2002). A family-wise error corrected $p < 0.05$ with a cluster-extent-based threshold of 10 or more voxels was considered statistically significant. Significant fixels/voxels were visualized using the mrview tool in MRtrix3.

Non-parametric permutation testing and connectivity-based fixel enhancement (CFE) (Raffelt et al., 2015) were applied to identify significant differences in fixel-based metrics. Using baseline age and sex as covariates, paired comparisons of metrics between three different time points (baseline, first follow-up visit, and second follow-up visit) were performed in patients with PD. We also performed a comparison in these metrics between patients with PD and healthy control subjects at baseline.

To analyze the association between longitudinal changes of fixel-based metrics and the corresponding modifications in clinical parameters, linear regression was implemented. The effect of aging was also assessed through regression analysis between age and fixel-based metrics. This analysis was conducted at baseline both in patients with PD and healthy control subjects, with sex as a covariate.

Voxel-based analysis was performed on both FA and MD using threshold-free cluster enhancement, which included voxel-based smoothing, statistical inference, and correction for multiple comparisons with default parameters (dh = 0.1, E = 0.5, H = 2) (Smith and Nichols, 2009)

3. Results

3.1. Longitudinal changes in clinical characteristics

Table 1 shows the longitudinal changes in the clinical characteristics—including disease severity, motor function, and quality of life—of the study patients. Significant changes were observed for MHY ($p < 0.001$), UPDRS total ($p < 0.001$), UPDRS II ($p < 0.001$), UPDRS III ($p < 0.01$), PDQ39 ($p < 0.001$), ADL ($p < 0.001$), and CDR ($p < 0.01$). Disease severity—as reflected by UPDRS total and MHY—showed a highly significant ($p < 0.001$) deterioration between the first and second follow-up examinations, which was conversely less pronounced ($p < 0.05$) from baseline to the first follow-up. Motor function—as reflected by UPDRS III – showed a significant deterioration between the first and second follow-up examinations, but not from baseline to the first follow-up. A worsening over the former time points was also observed for PDQ39 and ADL ($p < 0.001$). ADL was found to deteriorate between the second and first follow-up visits ($p < 0.001$).

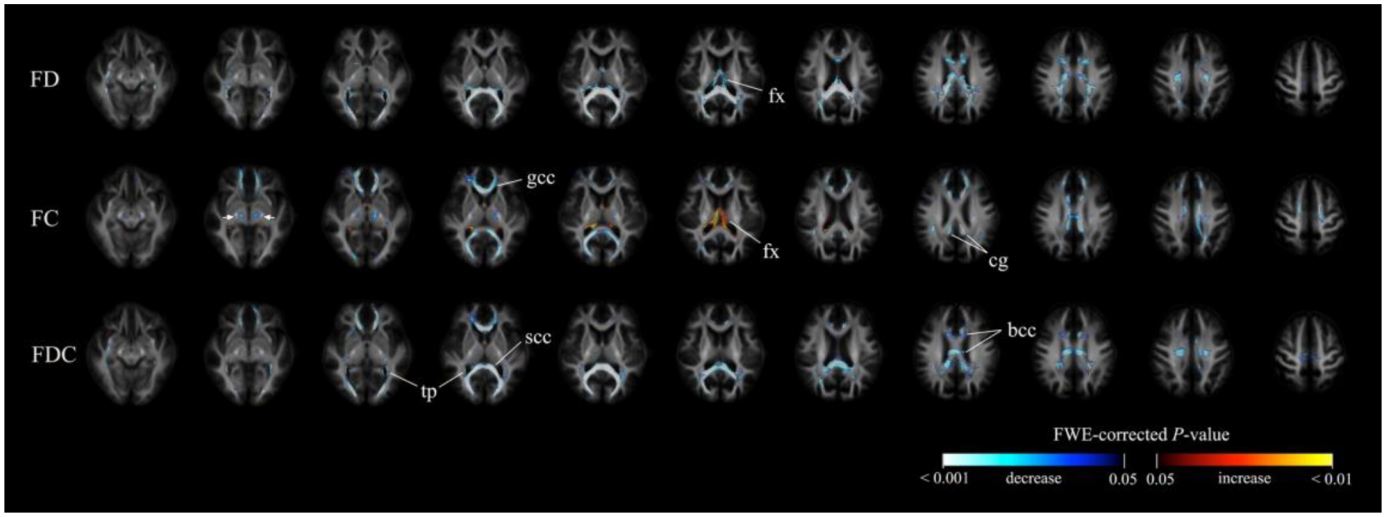

Fig. 3. Significant changes in fixel-based metrics between the second follow-up assessment and baseline. Significant fixels (family-wise error corrected p < 0.05) between the second follow-up assessment and baseline were displayed in the axial slices. They were colored according to p-values. Cold colors denote reduction, whereas warm colors denote increase. Top row: fiber density (FD) map; Middle row: fiber-bundle cross-section (FC) map; Bottom row: fiber density and cross-section (FDC) map. fx: fornix; gcc: genu of corpus callosum; cg: cingulum; tp: tapetum; scc: splenium of corpus callosum; bcc: body of corpus callosum.

3.2. Changes in white matter over time

No significant differences between patients with PD and healthy control subjects can be detected in baseline, neither from fixel-based analysis nor in conventional voxel-based analysis.

Fig. 2 shows the course of white matter degeneration over time. Areas of significant changes (family-wise error-corrected $p < 0.05$) for each fixel-based metric at different time points are depicted. Reductions in FD and FDC occurred earlier during the course of disease and predominantly affected the splenium of corpus callosum. In contrast, FC reductions were initially identified in the prefrontal regions, and an increase of FC was solely observed in fornix. To clearly illustrate the differences between the second follow-up assessment and baseline for each fixel-based metric, significant variations along fixels were plotted in axial slices (Fig. 3).

3.2.1. FDC variations over time

When data obtained on the second follow-up assessment were compared with baseline, we found that main FDC reductions were in the splenium, body and genu of corpus callosum—with an extension to the major and minor forceps and bilateral tapetum. Other areas of significant FDC reduction included bilateral cingulum; posterior thalamic radiation; anterior, superior, and right posterior corona radiata; retrolenticular part of internal capsule; sagittal stratum; superior longitudinal fasciculus; right external capsule; right cerebral peduncle; and right uncinate fasciculus. Notably, FDC reductions in the splenium and major forceps occurred early between the first follow-up assessment and baseline, with further lowering being evident thereafter (i.e., between the second and first follow-up assessments). Between the first and second follow-up assessments, we noticed late FDC reductions in the genu of corpus callosum, right tapetum, and posterior thalamic radiation.

3.2.2. FD variations over time

The main FD reductions were identified in the splenium and body of corpus callosum, major forceps, tapetum, and fornix. Other areas of significant FD reduction included the bilateral retrolenticular part of internal capsule; posterior thalamic radiation; posterior, anterior and superior corona radiata; superior longitudinal fasciculus; right external capsule; left cingulum; bilateral sagittal stratum; and genu. Between the first follow-up assessment and baseline, FD showed reductions in the splenium, bilateral major forceps, tapetum, and sagittal stratum, with further lowering being evident thereafter. Between the first and second follow-up assessments, we noticed FD reductions in the fornix, right retrolenticular part of internal capsule, bilateral posterior corona radiata, and body of corpus callosum.

3.2.3. FC variations over time

Significant FC reduction were identified in the bilateral anterior part of superior frontal blade (Oishi et al., 2008); splenium, genu, and body of corpus callosum; major and minor forceps; cerebral peduncle; posterior and left retrolenticular parts of internal capsule; superior and anterior corona radiata; cingulum; superior longitudinal fasciculus; and posterior thalamic radiation. Increases of FC were identified in the bilateral fornix and tapetum. Early FC reduction (i.e., occurring between the first follow-up assessment and baseline) were evident for the anterior part of superior frontal blade, genu, and left cingulum. An increase of FC was found in the fornix. Between the second and first follow-up assessments, areas of FC reduction were identified in the splenium and right posterior thalamic radiation.

3.2.4. Significant fixels colored by direction

To shed more light on the differences between the second follow-up assessment and baseline, significant reduced fixels were displayed in representative slices (Fig. 4) (panels from a to d: FDC; panels from e to j: FC). Panel e depicts the differences between the first follow-up assessment and baseline. The FDC reduced regions were displayed in an axial view (panels a and b)—including the genu and splenium of corpus callosum, as well as the minor forceps, major forceps and cingulum. The FDC changes in a representative coronal slice of the splenium and tapetum (panel c) and in a representative sagittal view of the left cingulum and corpus callosum (panel d) are depicted. Changes in the left frontal white matter were evident between the first follow-up assessment and baseline (panel e), as well as between the second follow-up

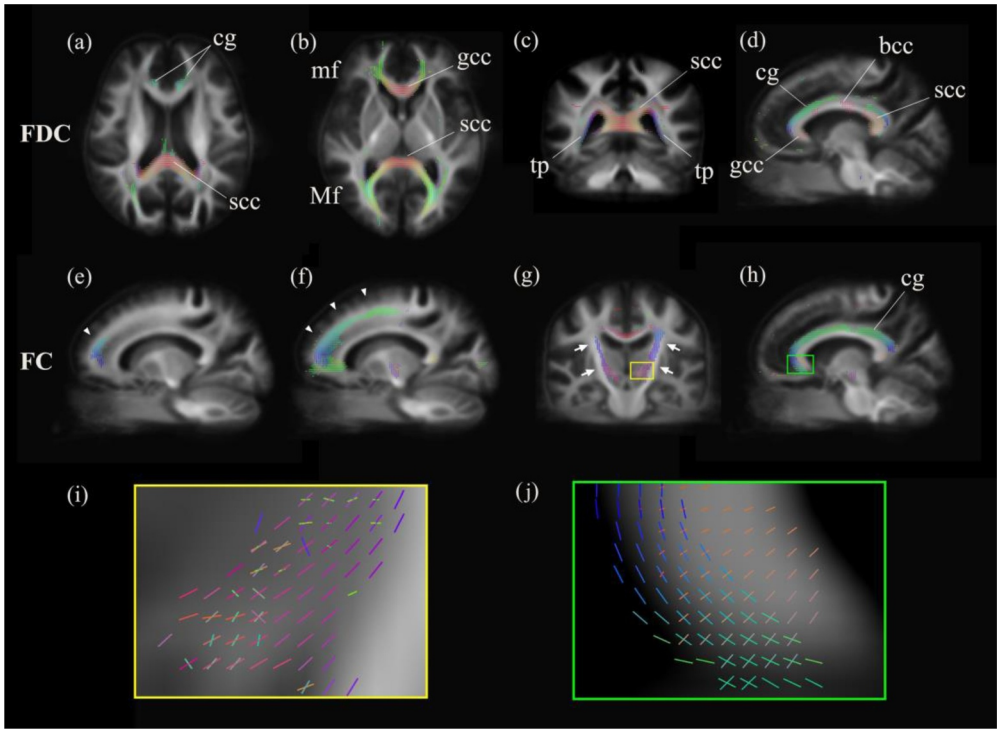

Fig. 4. Significant fixels colored by direction. Significant decreased fixels (family-wise error corrected $p < 0.05$) of fiber-bundle cross-section (FC) and fiber density and cross-section (FDC) between the second follow-up assessment and baseline (the only exception being (e)) were displayed in the axial (a, b), coronal (c, g), and sagittal (d–f, h) slices of a template map. They were colored according to the direction, as follows: anterior-to-posterior: green; superior-to-inferior: blue; and left-to-right: red. (e) and (f): Arrow heads point out the left frontal white matter changes between the first follow-up assessment and baseline ((e)) and the second follow-up assessment and baseline ((f)); (g): Arrows point out the hyperdirect pathways; (i): zoom in crossing-fiber area showed in (g); j: zoom in crossing-fiber area showed in (h). FD: fiber density; FC: fiber-bundle cross-section; FDC: fiber density and cross-section; cg: cingulum; scc: splenium of corpus callosum; mf: minor forceps; Mf: major forceps; gcc: genu of corpus callosum; tp: tapetum; bcc: body of corpus callosum. (For interpretation of the references to color in this figure legend, the reader is referred to the web version of this article.)

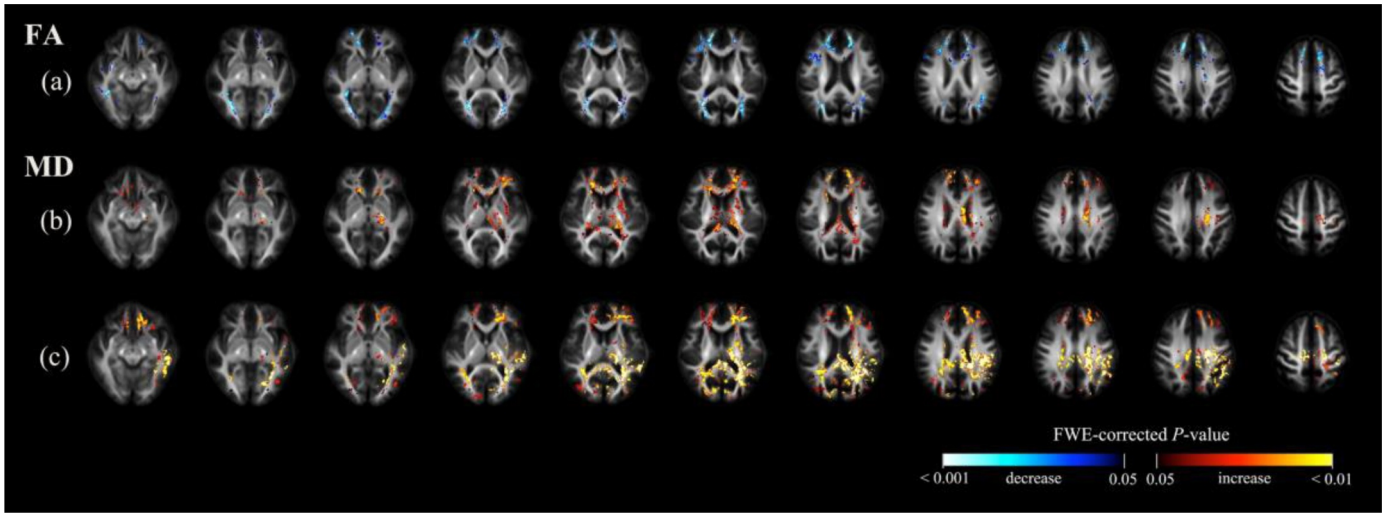

Fig. 5. Significant findings from voxel-based analysis. Significant voxels (family-wise error) corrected p < 0.05) were colored according to *p*-values, and displayed in the axial slices. Row (a): areas characterized by a significant decrease in fractional anisotropy (FA) between baseline and the second follow-up assessment; row (b): areas characterized by a significant increase in mean diffusivity (MD) between baseline and the first follow-up assessment; row (c): areas characterized by a significant increase in MD between baseline and the second follow-up assessment. FA did not show significant differences between baseline and the first follow-up assessment.

assessment and baseline (panel f). Enlarged regions characterized by the presence of crossing fibers are displayed in a coronal view within the hyperdirect pathway (panels i and g) and in a sagittal view within the left cingulum (panels j and h).

3.2.5. Voxel-based analysis over time

Fig. 5 shows the findings from voxel-based analysis over time. When data obtained at the second follow-up visit were compared with baseline, the main reductions in FA were identified in the posterior thalamic radiation, genu of corpus callosum, and tapetum. Other areas of FA reduction included the anterior corona, splenium, and sagittal stratum. (Fig. 5a). The main MD increases were identified in the splenium of corpus callosum; bilateral tapetum; anterior, superior, and posterior corona radiata; posterior thalamic radiation; cingulum; superior longitudinal fasciculus; left posterior limb of internal capsule; and left external capsule. Other areas of MD increase included the right posterior limb of internal capsule, left anterior limb of internal capsule and body of corpus callosum (Fig. 5c).

When we compared data from the first follow-up assessment to baseline, we failed to identify significant changes in FA. MD increases were found in body, splenium, and genu of corpus callosum; left external capsule; bilateral anterior, superior, and posterior corona radiata; anterior limb, posterior limb, and retrolenticular part of internal capsule; fornix, left cerebral peduncle, left cingulum, bilateral posterior thalamic radiation, tapetum, and left superior longitudinal fasciculus (Fig. 5b). We did not identify significant changes in terms of FA and MD between the second and first follow-up assessments.

3.3. Relationship between the longitudinal differences in clinical parameters and fixel-based metrics

Fig. 6 shows the associations between longitudinal differences in clinical parameters and fixel-based metrics. A reduction of FD in the splenium of corpus callosum and tapetum were associated with the increase of PDQ39. Positive associations of FC in the anterior part of the body of corpus callosum were observed with UPDRS total, UPDRS II, and UPDRS III. FC reduction in the body of corpus callosum (with an extension to the left superior corona radiata that tend to project into the primary motor cortex) was found to be associated with increase in UPDRS total and ADL. A similar association was observed for ADL in the right superior corona.

3.4. Temporal course of fixel-based metrics in FDC reduction areas

Fig. 7 showed how changes in FDC (Panel a) may stem from modifications in either FD (Panel b) or FC (Panel c). Seven regions of interest, including genu, body, splenium of corpus callosum, bilateral tapetum and cingulum—as highlighted in Fig. 4—was reported.

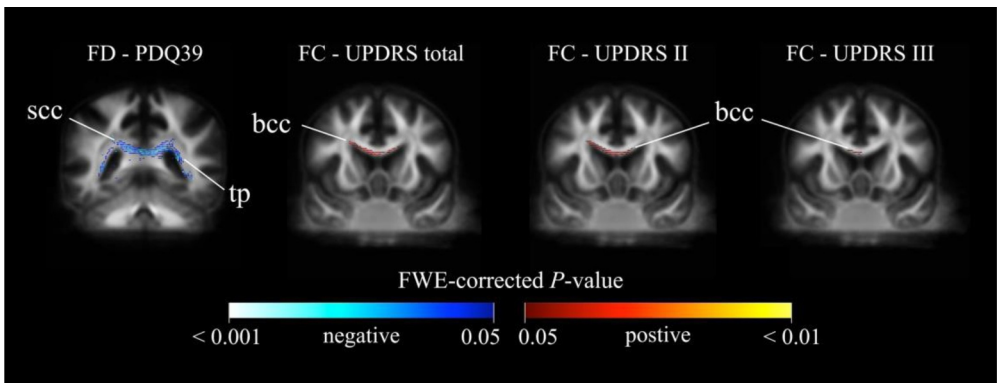

Fig. 6. Relationship between the longitudinal differences in clinical parameters and fixel-based metrics. Fixel-wise regression analysis was performed to identify the associations between longitudinal differences in clinical parameters and fixel-based metrics. Significant fixels (family-wise error corrected $p < 0.05$) were colored according to *p*-values and displayed in coronal view. Warm colors denote positive associations, whereas cold colors denote inverse relationships. FD: fiber density; FC: fiber-bundle cross-section; PDQ39: 39-item Parkinson's Disease Questionnaire; UPDRS: Unified Parkinson's Disease Rating Scale; scc: splenium of corpus callosum; tp: tapetum; bcc: body of corpus callosum.

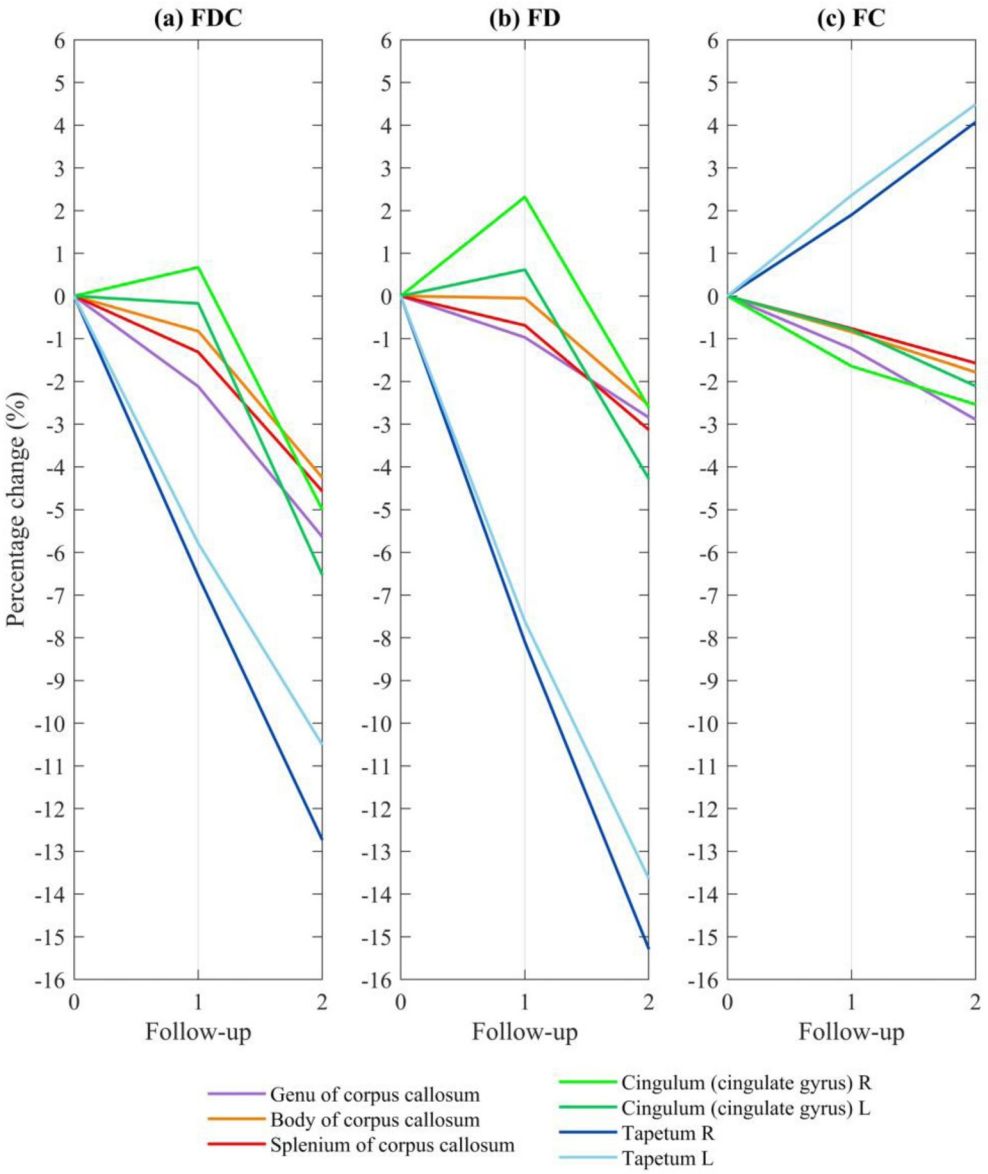

Fig 7. Temporal course of fixel-based metrics in areas showing FDC reduction. Fig. 7 shows how FDC changes (panel a) could stem from variations in either FD (panel b) or FC (panel c). Fixels showing a significant decrease in FDC (family-wise error corrected $p < 0.05$) between the second follow-up and baseline were identified, from which both FD and FC were extracted. The average fixel-based metrics were expressed as percentage changes after normalization for baseline values. Seven regions of interest–including genu, body and splenium of corpus callosum, bilateral cingulum and tapetum—are reported. FDC: fiber density and cross-section; FD: fiber density; FC: fiber-bundle cross-section.

Additional regions can be found in Supplementary Fig. 1.

Reductions in both FD and FC were observed in the genu, body, and splenium of corpus callosum. The declines were more pronounced between the second and first follow-up assessments. The bilateral tapetum showed a diverging pattern of decreased FD and increased FC over time, which ultimately led to an FDC reduction. FD in bilateral cingulum increased in the first and decreased in the second follow-up. Counterbalanced by a steadily decreased FC, FDC in left cingulum steadily decreased but right cingulum underwent an increase follow by a reduction over time.

3.5. Relationship between fixel-based metrics and age

We noticed the existence of an age-related white matter degeneration, and the patterns were different between patients with PD and healthy control subjects. Negative associations with age were more prominent in patients with PD than in healthy control subjects (Fig. 8). In healthy control subjects, FDC and FC did not show any significant associations with age. Positive associations between FD and age were found in the bilateral posterior limb of internal capsule, right superior corona radiata, and left cingulum. Negative associations were observed in the bilateral fornix, tapetum, sagittal stratum, body and splenium of corpus callosum, and posterior corona radiata.

In PD patients, we did not identify positive associations between fixel-based metrics and age. Negative associations with FD were observed in the bilateral fornix, genu and splenium of corpus callosum, tapetum, and sagittal stratum. With regard to FC, negative associations were found in the bilateral cingulum, anterior corona radiata, left sagittal stratum, and left fornix. As far as FDC is concerned, the main associations were identified in the splenium of corpus callosum, bilateral fornix, and tapetum. Other associations were found in the posterior corona radiate, left posterior thalamic radiation, and left sagittal stratum.

4. Discussion

4.1. Major findings

This study provides a thorough FBA profile of longitudinal white matter alterations occurring in patients with PD. The major longitudinal reductions in white matter were observed in the splenium of corpus callosum – in which such changes occurred in an earlier phase and were

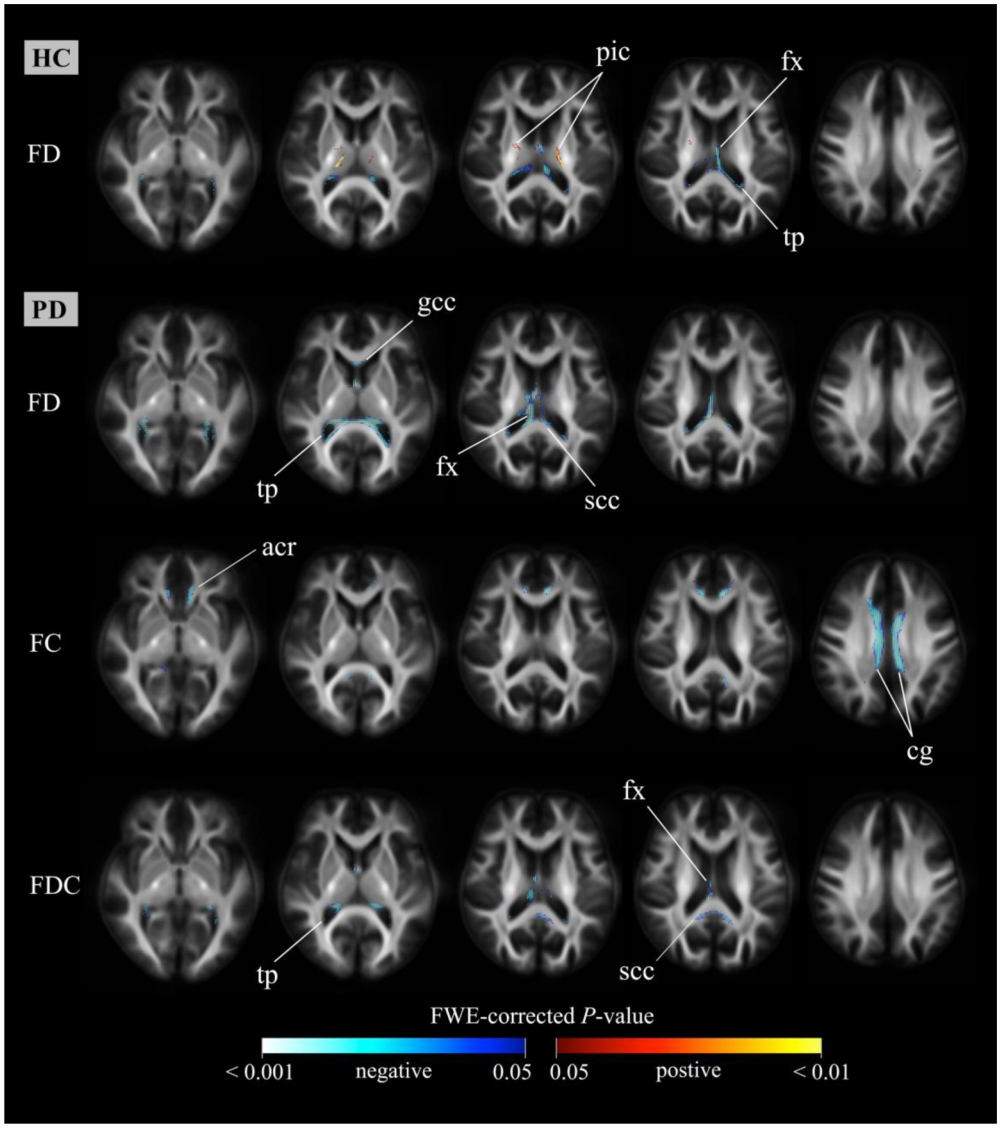

Fig. 8. Relationship between fixel-based metrics and age. We performed fixel-wise regression analysis between age and baseline fixel-based metrics in both patients with PD and healthy control subjects. Family-wise error (FWE)-corrected p values ($p < 0.05$) were used. Significant fixels are shown using streamline points and colored p-values. In healthy control subjects, FDC and FC did not show any significant associations with age. Positive associations were not observed in patients with PD. Warm colors denote positive associations, whereas cold colors denote inverse associations. PD: Parkinson's disease; HC: healthy control; FD: fiber density; FC: fiber-bundle cross-section; FDC: fiber density and cross-section; pic: posterior internal capsule; fx: fornix; tp: tapetum; gcc: genu of corpus callosum; scc: splenium of corpus callosum; acr: anterior corona radiata, cg: cingulum.

characterized by a more pronounced progression over time. Reductions of FD and FDC in the splenium were already evident between the first follow-up assessment and baseline, whereas FC was found to decrease only between the second and first follow-up assessment. These observations suggest that the first manifestations of white matter degeneration in the splenium might be related to axonal degeneration, which was subsequently followed by fiber bundle atrophy (Raffelt et al., 2017). Furthermore, a decrease of FD in splenium of the corpus callosum was related to a significant deterioration of PDQ39.

Herein, we showed that white matter changes occurring in the splenium and other commissural areas do evolve over time. These data may pave the way towards novel preventive and diagnostic strategies.

4.2. Early white matter damage in commissural areas were found to progress over time

We noticed early degeneration of white matter in the splenium of corpus callosum and other commissural areas (e.g., genu, body of corpus callosum and tapetum). The splenium could be a key area controlling verbal fluency (Hines et al., 1992) – which is frequently impaired in early-stage PD (Azuma et al., 2003; Domellöf et al., 2015). Using tract-based specific statistics, a previous study conducted in early-to-mid-stage patients described an involvement of the right splenium—which was correlated with disease severity (Rae et al., 2012). In our study, the decrease of FDC over time was paralleled by a deterioration of disease severity. The reduction of FD in splenium of the corpus callosum was found to be associated to PDQ39—a measure of subjective quality of life that includes mood, activities of daily living, motor function, and cognitive levels (Schrag et al., 2000). Our data indicate an early involvement of the splenium during the course of PD, which may potentially become a diagnostic and preventive target.

We identified reduction of FC in the genu and body of corpus callosum between the first follow-up assessment and baseline. Notably, abnormalities of the genu have been related to cognitive dysfunction in patients with PD and dementia (Kamagata et al., 2013a). Our finding indicate that alterations of white matter occur early during the course of PD. Interestingly, the decrease of FC in the genu—reflecting atrophy—preceded that of FD. However, a stable MMSE in our patients was observed over time. More detailed cognitive testing is recommended in future research.

The body of corpus callosum—through which the transcallosal motor fibers transit—is a crucial motor-related area that is pathogenetically involved in PD (Galantucci et al., 2014). Here, we have shown that FC reduction occurring in this region was associated with a worsening of disease severity (UPDRS total) and daily self-care activities (ADL) in our patients with PD. However, we also observed that FC increased in anterior part of body of corpus callosum were associated to the deterioration of disease severity and motor function (UPDRS III). A

time-related deterioration of these parameters indicates that an increased FC may also capture the degenerative process occurring in the white matter. The disruption occurring in the body of corpus callosum highlights the relevance of white matter involvement in motor dysfunction occurring in PD.

The tapetum—which consists of extended fibers that cross the splenium—is structurally connected to the temporal lobe (Yakar et al., 2018). A previous voxel-based morphometry study in early-stage PD revealed that subcortical white matter alterations in the temporal lobe preceded grey matter changes (Martin et al., 2009). In this study, the tapetum showed an FD decrease from baseline to the first follow-up assessment, followed by an FDC reduction from the first to the second follow-up assessment. In areas of significant FDC decrease within the tapetum, a decreased FD and an increased FC were evident (Fig. 7). While FC increased was reported in developmental children (Genc et al., 2017), the histologic mechanism was still unclear. A reduced FD accompanied by an increased FC can be attributed to an enlargement in the extra-axonal matrix, which can increase as a consequence of inflammation, cell injury, or gliosis in the white matter (Raffelt et al., 2017), as that occurring in white matter edema (Assaf and Pasternak, 2008). However, further studies are required to confirm this possibility.

4.3. FC-predominant regions: hyperdirect pathway, superior frontal blade, and cingulate bundles

Here, we identified FC-predominant regions as related to the pathogenesis of PD—including the subthalamic nucleus region and the motor cortex, the superior frontal blade, and bilateral cingulate bundles. These regions formed part of the hyperdirect pathway (Nambu et al., 2002). A tract characterized by FC reduction (Fig. 4g) was identified through the cerebral peduncle, the posterior limb of internal capsule, and the superior corona radiata—which formed part of the hyperdirect pathway containing the corticobulbar tract, the corticospinal tract, and the thalamocortical tract (Wakana et al., 2004) projecting to the motor cortex. The significant reduction of FC—rather than of FD—indicates that the degenerative process within this pathway is chiefly driven by white matter atrophy. Notably, the association between a decreased FC and the increase of UPDRS total suggests that this pathway may be involved in the deterioration of disease severity over time. A significant decrease in FC from baseline to both follow-up assessments was also evident in the superior frontal blade—which may reflect an atrophic process affecting the mesocortical pathways in the frontal white matter (Fig. 4e, f) (Bohnen et al., 2009; Rodriguez-Oroz et al., 2009).

Alterations of the cingulate bundle in patients with PD have been previously related to cognitive dysfunction and dementia (Matsui et al., 2007) as well as depression (Matsui et al., 2006). In our study, the cingulum region was characterized by a more pronounced reduction of FC (Fig. 4h) as a reflection of general bundle atrophy.

4.4. Comparison of FBA with voxel-based analysis and other diffusion imaging studies

Regions in our study characterized by a decrease of FA and an increase of MD were generally consistent with those areas showing changes of FDC (e.g., splenium and genu of corpus callosum, tapetum, corona radiata, and posterior thalamic radiation). However, FDC identified additional areas—such as the retrolenticular part of the internal capsule and left cerebral peduncle. Our findings suggest that FBA may be more sensitive and specific to changes in white matter structure as compared to voxel-based analysis. The detection by FBA might provide additional information related to white matter changes than conventional voxel-based analysis (Raffelt et al., 2017) and may shed more light to the pathology of PD—based on previous studies in the field.

Significant reductions of mean kurtosis have been reported in patients with PD, in whom they may serve as diagnostic biomarkers (Wang et al., 2011). Changes in white matter were observed in the corona radiata, superior longitudinal fasciculus, corpus callosum (genus, body, and splenium), internal capsule, external capsule, and cingulate fibers (Kamagata et al., 2014; Kamagata et al., 2013b; Weingarten et al., 2015). These data are consistent with our findings related to FC.

The diffusion from free-water components has been shown to increase in the substantia nigra of patients with PD and has been related to disease progression (Burciu et al., 2017; Planetta et al., 2015). Similarly, an increase of free-water diffusion in white matter (such as in the cerebellar peduncle and corpus callosum) has been reported in atypical PD (Andersson and Sotiropoulos, 2015). The motor pathways degeneration—as reflected by changes in FC observed in our study – may explain the connection between the dopaminergic system of the substantia nigra and white matter dopaminergic pathways (Chu et al., 2017). In summary, the white matter changes identified by our current fixel-based analysis are in line with the results obtained in previous diffusion studies of PD.

4.5. Temporal alternations of fixel-based metrics

The longitudinal changes of white matter identified in this study varied according to time and regions. For example, FDC steadily decreased in corpus callosum, whereas it showed a temporary increase followed by a decrease in right cingulum (Fig. 7)

Temporary increases in FDC were observed in the right cingulum (Fig. 7a), in addition to retrolenticular part of internal capsule, and corona radiata (Supplementary Fig. 1). A dynamic balance may occur in the white matter microenvironment. Longitudinal assessments over time may cast light on how diffusion MRI indices can vary according to the progression of patients with PD. In our study, the temporary increase of FDC could be attributed to a temporary change in FD counterbalanced by an increase in FC. Because FD increased in the first and decreased in the second follow-up, These temporary changes seem to suggest that variations in diffusion MRI-derived indices are neither static nor monotonic—potentially offering an explanation for the discrepant findings from the cross-sectional literature (Atkinson-Clement et al., 2017; Bohnen and Albin, 2011). Future longitudinal studies should benefit from different multiple follow-up assessments, which should help capture in greater detail how the temporal pattern of these transient changes.

Noticeably no significant differences can be detected between patients and healthy control subjects in baseline, using both fixel-based and voxel-based analyses. Cross-sectional studies which focused on white matter of the (1) whole brain (Rolheiser et al., 2011; Wen et al., 2016), (2) corpus callosum (Guimarães et al., 2018; Ito et al., 2008; Kamagata et al., 2013a; Wiltshire et al., 2010), or (3) cingulum (Guimarães et al., 2018; Wiltshire et al., 2010) did not identify significant differences between patients with PD and healthy control subject as in our results. This observation might partially be attributed to the fact that all these studies were conducted in patients at a relatively early-stage (MHY 1-2.5 or UPDRS III < 30).

4.6. Aging effects in white matter degeneration

Because no follow-up examinations were performed in healthy control subjects in our study, consequently, we cannot rule out an interaction between the disease and normal aging. However, we observed that patients with PD and healthy control subjects were different with regard to age-related white matter degeneration, suggesting the existence of a PD-specific aging process.

In healthy control subjects, only FD decreased with age, such as fornix, tapetum, splenium, and sagittal stratum. Because these regions were prominently affected in patients with PD, we speculate that PD

may facilitate physiological age-induced degeneration in these regions. In contrast, additional reduction in both FDC and FC can be noticed, which were inversely associated with age in patients of PD. Notably, regions showing baseline age-related alterations in patients with PD were also found to deteriorate at follow-up, the only exception being FC of the posterior corona radiata and left sagittal stratum. This observation might support our longitudinal findings.

In previous studies focusing on healthy subjects in the age range of our study participants, discrepancies across studies were evident. For example, FA in splenium of corpus callosum was reported to be increased (Michielse et al., 2010), decreased (Kennedy and Raz, 2009), or stable (Hsu et al., 2010) as the subjects aged. FA in body of corpus callosum was reported to be either decreased (Hsu et al., 2010; Ota et al., 2006) or stable (Michielse et al., 2010). However, the FA in genu of corpus callosum (Kennedy and Raz, 2009; Michielse et al., 2010; Ota et al., 2006) and fornix were consistently reported to decrease with aging (Jang et al., 2011; Michielse et al., 2010).

Taken together, genu of corpus callosum and fornix might degenerate with aging. Our current findings also indicate that these two regions – in addition to other areas – may show a PD-facilitated aging process.

4.7. Limitations and future directions

Our findings should be interpreted in the context of some caveats. For example, the cognitive tests in our study (i.e., MMSE and CDR) may not be sensitive or specific enough for the mild cognitive changes in patients with PD (Lessig et al., 2012). Future studies using appropriate cognitive tests – including the Montreal cognitive assessment (MoCA) – are necessary to examine the cognitive effect of white matter degeneration occurring in PD. In addition, the majority of the study patients had early-stage PD. Additional fixel examinations with extended follow-up periods may help to understand the long-term PD-specific white matter degenerative course.

5. Conclusion

By using fixel-based analysis, this study described the longitudinal patterns of white matter degeneration occurring in patients with PD. Our data lend further support to the key pathophysiological role played by white matter in the pathogenesis of PD. Importantly, we identified FC as a PD-related metric.

Funding

This work was financially supported by the Ministry of Science and Technology of Taiwan (grant MOST 106–2314-B-182 -018 -MY3, MOST 106-2911-I-182-505, MOST 107-2911-I-182-503, NMRP 96–2314-B-182A-071), the Healthy Aging Research Center (grant EMRPD1H0411, EMRPD1H0551, EMRPD1H0431, EMRPD1I0501, EMRPD1I0471), and the Chang Gung Memorial Hospital (grants CIRPD1E0061-3, CMRPD3D0011-3, CMRPD1C0291-3, CMRPD1G0561-2, and CMRPG2B0251).

Declaration of Competing Interest

None.

Acknowledgments

This work was supported by the Imaging Core Laboratory of the Institute for Radiological Research and the Center for Advanced Molecular Imaging and Translation. The authors wish to acknowledge the Neuroscience Research Center (Chang Gung Memorial Hospital), the Healthy Aging Research Center (Chang Gung University), and the Division of Chinese Acupuncture and Traumatology (Linkou Chang Gung Memorial Hospital) for their invaluable help. JDT was supported by the Wellcome/EPSRC Centre for Medical Engineering at King's College London [WT 203148/Z/16/Z] and the National Institute for Health Research (NIHR) Biomedical Research Centre at Guy's and St Thomas' NHS Foundation Trust and King's College London. The views expressed are those of the author(s) and not necessarily those of the NHS, the NIHR or the Department of Health.

Supplementary materials

Supplementary material associated with this article can be found, in the online version, at doi:10.1016/j.nicl.2019.102098.

References

Andersson, J.L., Sotiropoulos, S.N., 2015. Non-parametric representation and prediction of single- and multi-shell diffusion-weighted MRI data using Gaussian processes. Neuroimage 122, 166–176.
Andersson, J.L.R., Sotiropoulos, S.N., 2016. An integrated approach to correction for off-resonance effects and subject movement in diffusion MR imaging. Neuroimage 125, 1063–1078.
Assaf, Y., Pasternak, O., 2008. Diffusion tensor imaging (DTI)-based white matter mapping in brain research: a review. J. Mol. Neurosci. 34, 51–61.
Atkinson-Clement, C., Pinto, S., Eusebio, A., Coulon, O., 2017. Diffusion tensor imaging in Parkinson's disease: review and meta-analysis. NeuroImage Clin. 16, 98–110.
Azuma, T., Cruz, R.F., Bayles, K.A., Tomoeda, C.K., Montgomery, E.B., 2003. A longitudinal study of neuropsychological change in individuals with Parkinson's disease. Int. J. Geriatr. Psychiatry 18, 1043–1049.
Bach, M., Laun, F.B., Leemans, A., Tax, C.M.W., Biessels, G.J., Stieltjes, B., Maier-Hein, K.H., 2014. Methodological considerations on tract-based spatial statistics (TBSS). Neuroimage 100, 358–369.
Bohnen, N.I., Albin, R.L., 2011. White matter lesions in Parkinson disease. Nat. Rev. Neurol. 7, 229.
Bohnen, N.I., Bogan, C.W., Müller, M.L.T.M., 2009. Frontal and periventricular brain white matter lesions and cortical deafferentation of cholinergic and other neuromodulatory axonal projections. Eur. Neurol. J. 1, 33–50.
Braak, H., Tredici, K.D., Rüb, U., de Vos, R.A.I., Jansen Steur, E.N.H., Braak, E., 2003. Staging of brain pathology related to sporadic Parkinson's disease. Neurobiol. Aging 24, 197–211.
Brooks, D.J., 2010. Imaging Approaches to Parkinson Disease. J. Nucl. Med. 51, 596–609.
Burciu, R.G., Ofori, E., Archer, D.B., Wu, S.S., Pasternak, O., McFarland, N.R., Okun, M.S., Vaillancourt, D.E., 2017. Progression marker of Parkinson's disease: a 4-year multi-site imaging study. Brain J. Neurol. 140, 2183–2192.
Chu, H.-Y., McIver, E.L., Kovaleski, R.F., Atherton, J.F., Bevan, M.D., 2017. Loss of hyperdirect pathway cortico-subthalamic inputs following degeneration of midbrain dopamine neurons. Neuron 95, 1306–1318.e1305.
Damier, P., Hirsch, E., Agid, Y., Graybiel, A., 1999. The substantia nigra of the human brain: II. Patterns of loss of dopamine-containing neurons in Parkinson's disease. Brain 122, 1437–1448.
Domellöf, M.E., Ekman, U., Forsgren, L., Elgh, E., 2015. Cognitive function in the early phase of Parkinson's disease, a five-year follow-up. Acta Neurol. Scandi. 132, 79–88.
Fahn, S., Elton, R., Committee, U.D., 1987. Unified Parkinson's disease rating scale. In: Fahn, S., Marsden, C.D., Calne, D., Goldstein, M. (Eds.), Recent Developments in Parkinson's Disease 2. Macmillan Healthcare Information, Florham Park, NJ, pp. 153–163.
Galantucci, S., Agosta, F., Stankovic, I., Petrovic, I., Stojkovic, T., Comi, G., Kostic, V., Filippi, M., 2014. Corpus Callosum Damage and Motor Function in Parkinson's Disease (P2. 006). AAN Enterprises.
Genc, S., Seal, M.L., Dhollander, T., Malpas, C.B., Hazell, P., Silk, T.J., 2017. White matter alterations at pubertal onset. Neuroimage 156, 286–292.
Goetz, C.G., Poewe, W., Rascol, O., Sampaio, C., Stebbins, G.T., Counsell, C., Giladi, N., Holloway, R.G., Moore, C.G., Wenning, G.K., 2004. Movement disorder society task force report on the Hoehn and Yahr staging scale: status and recommendations the movement disorder society task force on rating scales for Parkinson's disease. Mov. Disord. 19, 1020–1028.
Grazioplene, R.G., Bearden, C.E., Subotnik, K.L., Ventura, J., Haut, K., Nuechterlein, K.H., Cannon, T.D., 2018. Connectivity-enhanced diffusion analysis reveals white matter density disruptions in first episode and chronic schizophrenia. NeuroImage Clin. 18, 608–616.
Guimarães, R.P., Campos, B.M., de Rezende, T.J., Piovesana, L., Azevedo, P.C., Amato-Filho, A.C., Cendes, F., D'Abreu, A., 2018. Is diffusion tensor imaging a good biomarker for early Parkinson's disease? Front. Neurol. 9, 626.
Hines, M., Chiu, L., McAdams, L.A., Bentler, P.M., Lipcamon, J., 1992. Cognition and the corpus callosum: verbal fluency, visuospatial ability, and language lateralization related to midsagittal surface areas of callosal subregions. Behav. Neurosci. 106, 3.
Hsu, J.-L., Van Hecke, W., Bai, C.-H., Lee, C.-H., Tsai, Y.-F., Chiu, H.-C., Jaw, F.-S., Hsu, C.-Y., Leu, J.-G., Chen, W.-H., Leemans, A., 2010. Microstructural white matter changes in normal aging: A diffusion tensor imaging study with higher-order polynomial regression models. Neuroimage 49, 32–43.
Hughes, A.J., Daniel, S.E., Kilford, L., Lees, A.J., 1992. Accuracy of clinical diagnosis of idiopathic Parkinson's disease: a clinico-pathological study of 100 cases. J. Neurol.

Neurosurg. Psychiatry 55, 181–184.
Ito, S., Makino, T., Shirai, W., Hattori, T., 2008. Diffusion tensor analysis of corpus callosum in progressive supranuclear palsy. Neuroradiology 50, 981–985.
Jang, S.H., Cho, S.-H., Chang, M.C., 2011. Age-related degeneration of the fornix in the human brain: a diffusion tensor imaging study. Int. J. Neurosci. 121, 94–100.
Jang, S.H., Kwon, Y.H., Lee, M.Y., Kim, J.-R., Seo, J.P., 2016. Aging of the cingulum in the human brain: Preliminary study of a diffusion tensor imaging study. Neurosci. Lett. 610, 213–217.
Jeurissen, B., Tournier, J.-D., Dhollander, T., Connelly, A., Sijbers, J., 2014. Multi-tissue constrained spherical deconvolution for improved analysis of multi-shell diffusion MRI data. Neuroimage 103, 411–426.
Kamagata, K., Motoi, Y., Tomiyama, H., Abe, O., Ito, K., Shimoji, K., Suzuki, M., Hori, M., Nakanishi, A., Sano, T., Kuwatsuru, R., Sasai, K., Aoki, S., Hattori, N., 2013a. Relationship between cognitive impairment and white-matter alteration in Parkinson's disease with dementia: tract-based spatial statistics and tract-specific analysis. Eur. Radiol. 23, 1946–1955.
Kamagata, K., Tomiyama, H., Hatano, T., Motoi, Y., Abe, O., Shimoji, K., Kamiya, K., Suzuki, M., Hori, M., Yoshida, M., Hattori, N., Aoki, S., 2014. A preliminary diffusional kurtosis imaging study of Parkinson disease: comparison with conventional diffusion tensor imaging. Neuroradiology 56, 251–258.
Kamagata, K., Tomiyama, H., Motoi, Y., Kano, M., Abe, O., Ito, K., Shimoji, K., Suzuki, M., Hori, M., Nakanishi, A., Kuwatsuru, R., Sasai, K., Aoki, S., Hattori, N., 2013b. Diffusional kurtosis imaging of cingulate fibers in Parkinson disease: comparison with conventional diffusion tensor imaging. Magn. Reson. Imaging 31, 1501–1506.
Kellner, E., Dhital, B., Kiselev, V.G., Reisert, M., 2016. Gibbs-ringing artifact removal based on local subvoxel-shifts. Magn. Reson. Med. 76, 1574–1581.
Kendi, A.K., Lehericy, S., Luciana, M., Ugurbil, K., Tuite, P., 2008. Altered diffusion in the frontal lobe in Parkinson disease. Am. J. Neuroradiol. 29, 501–505.
Kennedy, K.M., Raz, N., 2009. Aging white matter and cognition: Differential effects of regional variations in diffusion properties on memory, executive functions, and speed. Neuropsychologia 47, 916–927.
Lessig, S., Nie, D., Xu, R., Corey-Bloom, J., 2012. Changes on brief cognitive instruments over time in Parkinson's disease. Mov. Disord. 27, 1125–1128.
Lo, C.-Y., Wang, P.-N., Chou, K.-H., Wang, J., He, Y., Lin, C.-P., 2010. Diffusion tensor tractography reveals abnormal topological organization in structural cortical networks in Alzheimer's disease. J. Neurosci. 30, 16876–16885.
Lu, C.-S., Ng, S.-H., Weng, Y.-H., Cheng, J.-S., Lin, W.-Y., Wai, Y.-Y., Chen, Y.-L., Wang, J.-J., 2016. Alterations of diffusion tensor MRI parameters in the brains of patients with Parkinson's disease compared with normal brains: possible diagnostic use. Eur. Radiol. 26, 3978–3988.
Malhotra, A., Sepehrizadeh, T., Dhollander, T., Wright, D., Castillo-Melendez, M., Sutherland, A.E., Pham, Y., Ditchfield, M., Polglase, G.R., de Veer, M., Jenkin, G., Pannek, K., Shishegar, R., Miller, S.L., 2019. Advanced MRI analysis to detect white matter brain injury in growth restricted newborn lambs. NeuroImage Clin. 24, 101991.
Martin, W.W., Wieler, M., Gee, M., Camicioli, R., 2009. Temporal lobe changes in early, untreated Parkinson's disease. Mov. Disord. 24, 1949–1954.
Matsui, H., Nishinaka, K., Oda, M., Niikawa, H., Komatsu, K., Kubori, T., Udaka, F., 2006. Depression in Parkinson's disease. J. Neurol. 254, 1170.
Matsui, H., Nishinaka, K., Oda, M., Niikawa, H., Kubori, T., Udaka, F., 2007. Dementia in Parkinson's disease: diffusion tensor imaging. Acta Neurol. Scandi. 116, 177–181.
Michielse, S., Coupland, N., Camicioli, R., Carter, R., Seres, P., Sabino, J., Malykhin, N., 2010. Selective effects of aging on brain white matter microstructure: a diffusion tensor imaging tractography study. Neuroimage 52, 1190–1201.
Mori, S., Oishi, K., Jiang, H., Jiang, L., Li, X., Akhter, K., Hua, K., Faria, A.V., Mahmood, A., Woods, R., Toga, A.W., Pike, G.B., Neto, P.R., Evans, A., Zhang, J., Huang, H., Miller, M.I., van Zijl, P., Mazziotta, J., 2008. Stereotaxic white matter atlas based on diffusion tensor imaging in an ICBM template. Neuroimage 40, 570–582.
Morris, J.C., 1993. The clinical dementia rating (CDR): current version and scoring rules. Neurology 43, 2412–2414.
Nambu, A., Tokuno, H., Takada, M., 2002. Functional significance of the cortico—subthalamo–pallidal 'hyperdirect'pathway. Neuroscience research 43, 111–117.
Nichols, T.E., Holmes, A.P., 2002. Nonparametric permutation tests for functional neuroimaging: a primer with examples. Hum. Brain Mapp. 15, 1–25.
Oishi, K., Zilles, K., Amunts, K., Faria, A., Jiang, H., Li, X., Akhter, K., Hua, K., Woods, R., Toga, A.W., Pike, G.B., Rosa-Neto, P., Evans, A., Zhang, J., Huang, H., Miller, M.I., van Zijl, P.C.M., Mazziotta, J., Mori, S., 2008. Human brain white matter atlas: identification and assignment of common anatomical structures in superficial white matter. Neuroimage 43, 447–457.
Ota, M., Obata, T., Akine, Y., Ito, H., Ikehira, H., Asada, T., Suhara, T., 2006. Age-related degeneration of corpus callosum measured with diffusion tensor imaging. Neuroimage 31, 1445–1452.
Peto, V., Jenkinson, C., Fitzpatrick, R., Greenhall, R., 1995. The development and validation of a short measure of functioning and well being for individuals with Parkinson's disease. Qual. Life Res. 4, 241–248.
Planetta, P.J., Ofori, E., Pasternak, O., Burciu, R.G., Shukla, P., DeSimone, J.C., Okun, M.S., McFarland, N.R., Vaillancourt, D.E., 2015. Free-water imaging in Parkinson's disease and atypical Parkinsonism. Brain 139, 495–508.
Rae, C.L., Correia, M.M., Altena, E., Hughes, L.E., Barker, R.A., Rowe, J.B., 2012. White matter pathology in Parkinson's disease: the effect of imaging protocol differences and relevance to executive function. Neuroimage 62, 1675–1684.
Raffelt, D., Tournier, J.D., Fripp, J., Crozier, S., Connelly, A., Salvado, O., 2011. Symmetric diffeomorphic registration of fibre orientation distributions. Neuroimage 56, 1171–1180.
Raffelt, D.A., Smith, R.E., Ridgway, G.R., Tournier, J.D., Vaughan, D.N., Rose, S., Henderson, R., Connelly, A., 2015. Connectivity-based fixel enhancement: whole-brain statistical analysis of diffusion MRI measures in the presence of crossing fibres. Neuroimage 117, 40–55.
Raffelt, D.A., Tournier, J.D., Smith, R.E., Vaughan, D.N., Jackson, G., Ridgway, G.R., Connelly, A., 2017. Investigating white matter fibre density and morphology using fixel-based analysis. Neuroimage 144, 58–73.
Rodriguez-Oroz, M.C., Jahanshahi, M., Krack, P., Litvan, I., Macias, R., Bezard, E., Obeso, J.A., 2009. Initial clinical manifestations of Parkinson's disease: features and pathophysiological mechanisms. Lancet Neurol. 8, 1128–1139.
Rolheiser, T.M., Fulton, H.G., Good, K.P., Fisk, J.D., McKelvey, J.R., Scherfler, C., Khan, N.M., Leslie, R.A., Robertson, H.A., 2011. Diffusion tensor imaging and olfactory identification testing in early-stage Parkinson's disease. J. Neurol. 258, 1254–1260.
Schrag, A., Jahanshahi, M., Quinn, N., 2000. What contributes to quality of life in patients with Parkinson's disease? J. Neurol. Neurosur. Amp Psych. 69, 308.
Schwab, R., England, A., Gillingham, F., Donaldson, M., 1969. Third symposium on Parkinson's disease. E. And S. Livingstone:, Edinburgh, pp. 152–157.
Smith, S.M., Nichols, T.E., 2009. Threshold-free cluster enhancement: addressing problems of smoothing, threshold dependence and localisation in cluster inference. NeuroImage 44, 83–98.
Tagliaferro, P., Burke, R.E., 2016. Retrograde axonal degeneration in Parkinson disease. J. Parkinson's Disease 6, 1–15.
Taylor, K.I., Sambataro, F., Boess, F., Bertolino, A., Dukart, J., 2018. Progressive Decline in Gray and White Matter Integrity in de novo Parkinson's Disease: An Analysis of Longitudinal Parkinson Progression Markers Initiative Diffusion Tensor Imaging Data. Front. Aging Neurosci. 10.
Tombaugh, T.N., McIntyre, N.J., 1992. The mini-mental state examination: a comprehensive review. J. Am. Geriatr. Soc. 40, 922–935.
Tustison, N.J., Avants, B.B., Cook, P.A., Zheng, Y., Egan, A., Yushkevich, P.A., Gee, J.C., 2010. N4ITK: improved N3 bias correction. IEEE Trans. Med. Imaging 29, 1310–1320.
Veraart, J., Novikov, D.S., Christiaens, D., Ades-aron, B., Sijbers, J., Fieremans, E., 2016. Denoising of diffusion MRI using random matrix theory. Neuroimage 142, 394–406.
Veraart, J., Sijbers, J., Sunaert, S., Leemans, A., Jeurissen, B., 2013. Weighted linear least squares estimation of diffusion MRI parameters: strengths, limitations, and pitfalls. NeuroImage 81, 335–346.
Wakana, S., Jiang, H., Nagae-Poetscher, L.M., Van Zijl, P.C., Mori, S., 2004. Fiber tract–based atlas of human white matter anatomy. Radiology 230, 77–87.
Wang, J.-J., Lin, W.-Y., Lu, C.-S., Weng, Y.-H., Ng, S.-H., Wang, C.-H., Liu, H.-L., Hsieh, R.-H., Wan, Y.-L., Wai, Y.-Y., 2011. Parkinson disease: diagnostic utility of diffusion kurtosis imaging. Radiology 261, 210–217.
Weingarten, C.P., Sundman, M.H., Hickey, P., Chen, N.-k., 2015. Neuroimaging of Parkinson's disease: Expanding views. Neurosci. Biobehav. Rev. 59, 16–52.
Wen, M.-C., Heng, H.S., Ng, S.Y., Tan, L.C., Chan, L.L., Tan, E.K., 2016. White matter microstructural characteristics in newly diagnosed Parkinson's disease: an unbiased whole-brain study. Sci. Reports 6, 35601.
Wiltshire, K., Concha, L., Gee, M., Bouchard, T., Beaulieu, C., Camicioli, R., 2010. Corpus callosum and cingulum tractography in Parkinson's disease. Canad. J. Neurol. Sci. 37, 595–600.
Yakar, F., Eroglu, U., Peker, E., Armagan, E., Comert, A., Ugur, H.C., 2018. Structure of corona radiata and tapetum fibers in ventricular surgery. J. Clin. Neurosci. 57, 143–148.
Zhan, W., Kang, G.A., Glass, G.A., Zhang, Y., Shirley, C., Millin, R., Possin, K.L., Nezamzadeh, M., Weiner, M.W., Marks Jr, W.J., 2012. Regional alterations of brain microstructure in Parkinson's disease using diffusion tensor imaging. Movement Disord. 27, 90–97.